PERGAMON

Acta mater. 48 (2000) 933–941

Acta MATERIALIA

www.elsevier.com/locate/actamat

NANOCRYSTALLINE Ni–3.6 at.% P AND ITS TRANSFORMATION SEQUENCE STUDIED BY ATOM-PROBE FIELD-ION MICROSCOPY

TH. HENTSCHEL†[1], D. ISHEIM[1]‡, R. KIRCHHEIM[1], F. MÜLLER[2] and H. KREYE[2]

[1]Institut für Metallphysik der Universität Göttingen, Hospitalstr. 3–7, D-37073 Göttingen, Germany and [2]Institut für Werkstofftechnik der Universität der Bundeswehr Hamburg, Holstenhofweg 85, D-22043 Hamburg, Germany.

(Received 7 June 1999; accepted 28 September 1999)

Abstract—The transformation sequence of electroless plated nanocrystalline Ni–3.6 at.% P layers upon different heat treatments is studied by means of differential scanning calorimetry (DSC), X-ray diffraction (XRD) and atom-probe field-ion microscopy (APFIM). APFIM reveals P segregation at the grain boundaries in the as-plated nanocrystalline alloy. DSC shows two heat releases upon isochronic heat treatment. During the first heat release, starting at about 136°C for a heating rate of 20°C/min, structural relaxation occurs first, followed by slight crystal growth and segregation enhancement, as shown by XRD and APFIM. Nucleation of the equilibrium phase Ni_3P starts in the transition to the second heat release. This second heat release, with a sharp onset at 417°C for heating at a rate of 20°C/min, is related to the major part of Ni_3P-phase formation and substantial grain growth. The transformation sequence is compared with the one observed on amorphous Ni–P alloys and discussed in terms of a thermodynamic model.

Keywords: Plating; Nanocrystalline materials; Nickel alloys; Grain growth; Segregation

1. INTRODUCTION

For more than a decade much attention has been drawn to metals and alloys with grain sizes in the nanometer range, so-called nanocrystalline materials. Due to the extremely large volume fraction of the interfacial area of grain boundaries in these materials, they exhibit unique mechanical, magnetic, electrical and corrosive properties [1, 2]. Numerous techniques have been developed to produce nanocrystalline materials, as described by Gleiter [1].

Nanocrystalline materials produced by various electrochemical plating methods are considered to be close to commercial application [3]. In particular, nickel–phosphorus (Ni–P) layers are superior contenders for corrosion and wear resistant coatings. By electroless plating (i.e. catalytic deposition by chemical reduction in aqueous solution), Ni–P layers with a P content between 2 and 20 at.% can be deposited on virtually any substrate material. Layers with nearly 20 at.% P which have been shown to be amorphous [4], have already been successfully used as commercial coatings [5, 6]. Recently, it has been found that nanocrystalline Ni–P layers, having a P content of only 2–8 at.%, exhibit a significantly higher wear resistance than layers with a higher content of P [7].

In order to understand the advantageous macroscopic properties of amorphous and nanocrystalline Ni–P layers, it is essential to characterize their microstructure on an atomic scale and since the as-plated material is far from thermodynamic equilibrium their thermal stability as well as their microstructural evolution during thermal treatment. Layers with P concentrations in the amorphous range have been investigated extensively, see, e.g. Refs [8–10] and references therein. While studies of grain growth [11, 12] and macroscopic properties [13] of nanocrystalline layers with lower P concentration have been published, there is less knowledge of the actual atomic-scale P distribution and its influence on the transformation behavior [13, 14].

In the present study, atom-probe field-ion microscopy (APFIM) has been chosen to characterize

† Present address: Institut für Werkstoffwissenschaften V, Universität Erlangen-Nürnberg, Martensstr. 7, D-91058 Erlangen, Germany.

‡ To whom all correspondence should be addressed. Present address: Materials Science and Engineering Department, Northwestern University, 2225 N. Campus Dr., Evanston, IL 60208, USA.

1359-6454/00/$20.00
PII: S1359-6454(99)00371-7

Table 1. Transformation states, respective heat treatments, characterization methods, and grain sizes as determined by X-ray diffraction

Transformation state	Heat treatment	Method	Grain size (nm) Ni(P)	Grain size (nm) Ni_3P
A	None (as plated)	XRD, FIM, AP	9	–
B	20°C/min to 250°C	XRD	11	–
B′	Isothermal 1 h 250°C	FIM, AP		–
C	20°C/min to 400°C	XRD	22	Phase present
C′	5°C/min to 400°C	FIM, AP		Phase present
D	20°C/min to 425°C	XRD, FIM, AP	33	25
E	20°C/min to 450°C	XRD, FIM, AP	78	34
F	20°C/min to 600°C	XRD	Microcryst.	Microcryst.

the microstructure and the local chemical composition of Ni–3.6 at.% P on the required atomic scale, both in the as-plated nanocrystalline state as well as after heat treatment. Differential scanning calorimetry (DSC) and X-ray diffraction analysis (XRD) are employed to follow the overall transformational behavior. We present evidence that both the as-plated microstructure and the transformation sequence of nanocrystalline Ni–P layers upon heat treatment are strongly correlated to the local distribution of P. It is also shown that the microstructural evolution upon thermal treatment of nanocrystalline Ni–P is closely related to the transformation sequence of amorphous Ni–P layers.

2. EXPERIMENTAL PROCEDURE

Layers of Ni–3.6 at.% P with a thickness of 40 μm were deposited by electroless plating onto a polished titanium substrate using a commercially available bath with a pH of 6.2 at a temperature of 70°C. The layers could be easily peeled off from the substrate and used as foils for further preparation and investigation. Electron microprobe analysis resulted in a mean P concentration of 3.58 ± 0.06 at.%. The transformation sequence was followed using a Perkin-Elmer DSC7 differential scanning calorimeter by recording the reaction enthalpies of the different steps of the transformation sequence during isochronal heating to 600°C with heating rates of 5 and 20°C/min. Grain sizes and the appearance of new phases were monitored after heating specimens at 20°C/min to selected temperatures using a Siemens D500 X-ray diffractometer with a Co-K_α source. FIM tips were prepared from as-plated foils as well as from heat-treated foils in a two-step procedure. First, strips cut from the layers were mechanically ground from the edges to parallelepipeds with a square cross section of about $40 \times 40\ \mu m^2$. To obtain FIM tips, the parallelepipeds were then electropolished in a solution of 10 vol.% perchloric acid in acetic acid. FIM imaging and AP analyses were performed using the APFIM described in Ref. [15]. For field-ion imaging, a mixture of 5×10^{-4} Pa neon and 1×10^{-5} Pa hydrogen was used. Atom-probe analyses were carried out using a pulse frequency of 10 Hz and a pulse fraction of 0.15–0.20 at a specimen temperature of 50 K. Table 1 lists the aging treatments, investigation methods employed, and designations of the respective transformation stages.

3. RESULTS

Isochronal heating at a rate of 20°C/min to 600°C yields the thermogram shown in Fig. 1. Two heating runs were performed under identical conditions, the second one being carried out with the completely transformed sample. In order to obtain the absolute heating power, the second run was subtracted from the first one. The result is shown in Fig. 1. This thermogram features two major exothermal transformation steps, indicated by the two heat releases I and II. Heat release I, very shallow, extends from an onset at about 136–380°C. The peak of heat release II, with an onset at 417°C and a peak temperature of 433°C, is very sharp, having a full width at half maximum (FWHM) of only 15°C. The observed onset temperatures correspond well with the values determined by Ref. [13] for electroless plated Ni–P layers with similar P contents using dilatometry and electric resistivity measurements. Heat release I amounts to an enthalpy of 2.2 kJ/g-atom and heat release II to

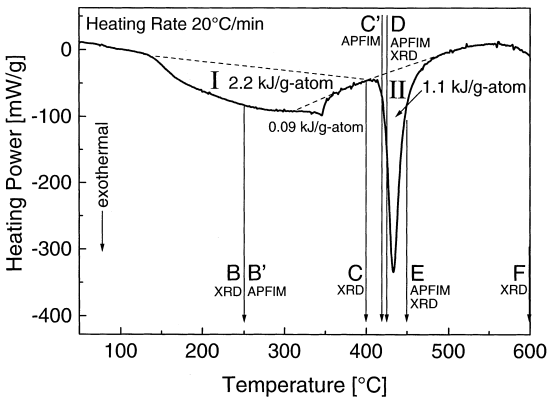

Fig. 1. Differential scanning calorimetry thermogram of nanocrystalline Ni–3.6 at.% P, recorded employing a heating rate of 20°C/min. The heat release of each exothermal process is indicated. The temperatures of transformation stages B, C, D, E, and F investigated by XRD and stages B′, C′, D, and E, investigated by APFIM, are indicated by arrows.

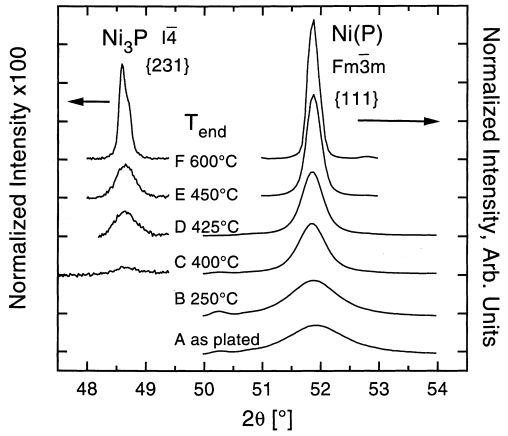

Fig. 2. X-ray diffractograms recorded for different transformation stages of initially nanocrystalline Ni–3.6 at.% P. The diagram displays the (111) reflection for Ni(P) and (231) for Ni_3P. The intensities are normalized taking the respective intensity of the Ni(P) reflection as 100%. Intensities for Ni_3P are magnified by 100 × .

1.1 kJ/g-atom. The small superimposed peak with a sharp edge at 346°C is due to endothermic magnetic disordering [16]. Because the magnetic peak occurs only in the second run, which is subtracted from the first one, it appears to be exothermal in Fig. 1. The edge of this peak at 346°C marks the Curie temperature of f.c.c. Ni-rich grains formed in the higher temperature range of the first run. This value is 12°C less than the value of 358°C reported as the Curie temperature for pure macrocrystalline Ni [17], probably due to the P content of the Ni-rich grains. Because the first run showed no distinct Curie temperature, the magnetic contribution is not included in the enthalpy of the first exothermal peak.

Isochronal heating at a rate of 5°C/min to 600°C results in the same transformation sequence with transformation onsets of 121°C for heat release I and 396°C for heat release II, with a peak temperature of 412°C. The shift to lower temperatures as a result of the smaller heating rate demonstrates that the transformations are thermally activated. In contrast, the magnetic disordering, having no activation barrier, exhibits with a measured Curie temperature of 345°C no variation of the transformation temperature upon change of the heating rate. Using the approach of Kissinger [18], an activation energy of 254 kJ/g-atom is found for the second peak. The first peak is too wide to match Kissinger's assumption of first-order annealing kinetics.

The transformation states investigated by XRD and APFIM are listed in Table 1 and marked in Fig. 1 to illustrate their position with respect to the observed two heat releases. State B′ is shown with state B at 250°C; state C′, created by heating at 5°C/min to 400°C, is located at the beginning of heat release II and is shown in Fig. 1 at a slightly higher temperature, taking into account the different heating rates.

The X-ray diffractograms shown in Fig. 2 illustrate grain growth and formation of the equilibrium Ni_3P phase upon heating at 20°C/min. The grain size was determined by the Scherrer formula employing the $K_{\alpha 2}$ correction. The results are summarized in Table 1. Heating to 250°C does not change the grain size significantly from the initial value of 9 nm in the as-plated material. At 400°C the grain size has doubled to 22 nm. Substantial grain growth starts at 425°C, with the grain diameter increasing from 34 to over 70 nm at 450°C. At 600°C, the microstructure is no longer nanocrystalline. Weak reflections of the Ni_3P phase could be observed after heating to 400°C, indicating the formation of a small volume fraction of Ni_3P. Heating to 425°C greatly increases the volume fraction and the size of the Ni_3P precipitates. From the FWHM of the much larger X-ray peak, the size of the Ni_3P precipitates could be determined, having almost reached the size of the nickel crystallites.

A comparison of the microstructural changes found by XRD with the reaction steps found in the thermogram shows heat release II to be related to the formation of the vast part of Ni_3P and substantial grain growth. For heat release I, XRD indicates moderate grain growth and limited formation of Ni_3P only in the high temperature part. Microstructural changes related to the low temperature part of heat release I up to 250°C could not be resolved by XRD. These changes were characterized applying APFIM, as detailed in the following.

The field-ion micrograph of an as-plated specimen, Fig. 3(a), top, resolves the nanocrystalline grain structure, as depicted schematically in Fig. 3(a), bottom. Individual grains appear as clusters of bright spots, with the grain boundaries appearing as dark lines. The chemical composition of a cylindrical volume about 2 nm in diameter was analyzed on atomic scale in depth, via selected-area atom-probe analysis, starting in the center of a grain. The result is exhibited in Fig. 4 in the form of an integral profile, that is, the cumulative number of P atoms detected vs the cumulative number of Ni atoms plus P atoms detected. The local slope of this diagram equals the local P concentration. The integral profile contains an almost atomically sharp transition from a region with 1.4 ± 0.8 at.% P to a region with 13.5 ± 3 at.% P having a length of about 1 nm. Figure 5(a) presents a concentration profile obtained by random-area atom-probe analysis of an as-plated specimen. The profile shows several peaks of P concentration above 10 at.% that clearly exceed the 2σ limits of the corresponding binomial distribution, thus confirming an inhomogeneous P distribution. The segregation concentration, averaged over the maxima of several concentration profiles, is 11 ± 2 at.% P; the average width of the segregation zones is 0.8 ± 0.1 nm. The typical peak distance of approximately 7 nm corresponds exactly with the characteristic length of the

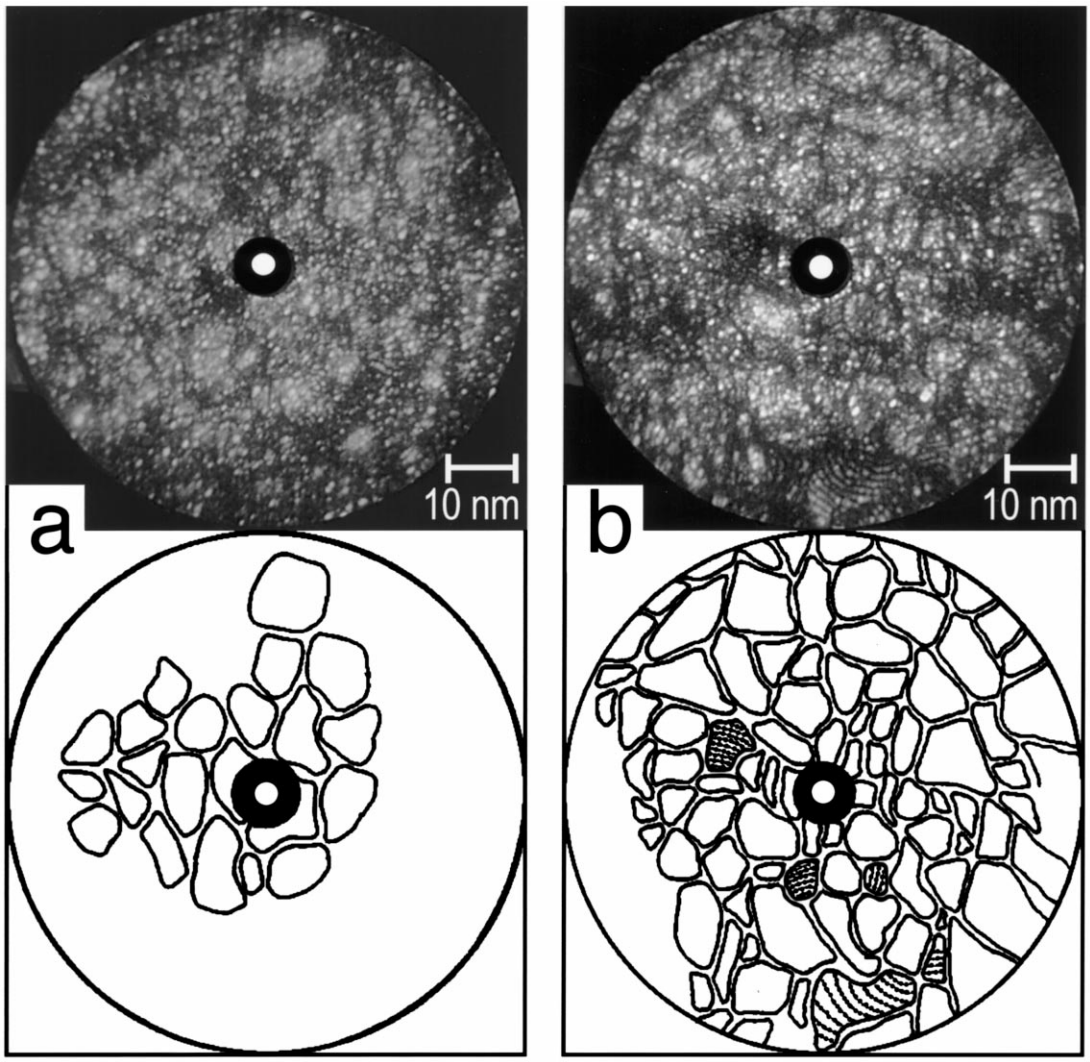

Fig. 3. Field-ion micrographs of initially nanocrystalline Ni–3.6 at.% P in different transformation stages: (a) as-plated; (b) isothermally aged at 250°C for 1 h; (c) isochronally heated at 5°C/min to 400°C; (d) isochronally heated at 20°C/min to 425°C; (e) isochronally heated at 20°C/min to 450°C. The schematic diagrams in the bottom parts of (a), (b), and (c) indicate the nanocrystalline grain structure.

nanocrystalline microstructure, i.e. the grain size of 9 nm, as determined by XRD†. The agreement of the mean distance of the segregation zones with the average grain size strongly suggests that the P segregation is related to the grain boundaries.

Figure 3(b), top, shows a field-ion image of a specimen after heat treatment B′: even after 1 h isothermal aging at 250°C, the grain size has hardly increased, in agreement with the XRD results obtained for state B. In Fig. 3(b), top, the grain boundaries, visible as dark lines, are more clearly resolved than in Fig. 3(a), top. The grain structure is depicted schematically in Fig. 3(b), bottom. For several grains, the crystalline structure becomes directly visible in Fig. 3(b), top, by the resolution of atomic terraces of crystallographic planes as indicated schematically in Fig. 3(b), bottom. Observation during continuous slow field evaporation reveals that grain boundaries and crystallographic planes are generally better resolved after heat treatment B′ than for the as-plated state.

The P distribution after 1 h isothermal aging at 250°C, exemplified by the random-area concentration profile displayed in Fig. 5(b), is very similar to the one observed for the as-plated state: the average segregation concentration is 12.5 ± 2 at.%, and the average width of the segregation zones does not differ significantly from the value determined for the as-plated state. Selected-area analyses of grains

† The average length of randomly chosen one-dimensional cuts through a spherical grain amounts to 2/3 of the grain diameter.

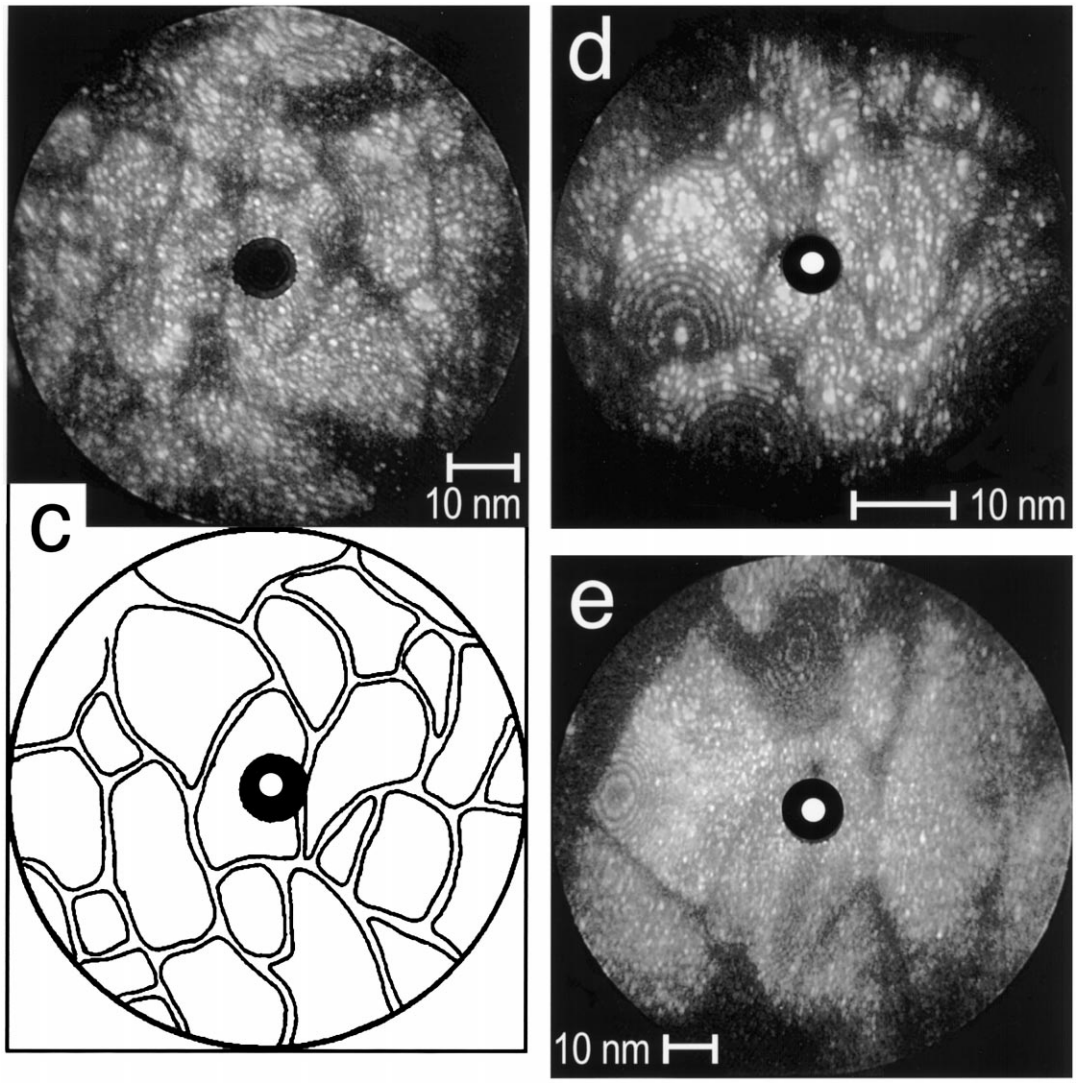

Fig. 3 (*continued*)

of material in state B′, similar to the one displayed for the as-plated state in Fig. 4, confirm, that the nanocrystalline grains are P depleted with respect to the overall mean P concentration, again suggesting that the P segregation is related to the grain boundaries. These observations indicate that the atomic P distribution has not changed considerably during heating treatment B′. Moreover, virtually no grain growth has been observed up to 250°C, as shown by XRD. However, the thermogram displayed in Fig. 1, shows a heat release of roughly 1 kJ/g-atom during heating to 250°C. As grain size and solute distribution remain essentially unchanged, the heat release is attributed to structural relaxations such as annihilation of point defects and dislocations within grains and grain boundary zones. This is in agreement with the observation of more clearly resolved grain boundaries and crystallographic planes in FIM micrographs after heat treatment B′ as shown in Fig. 3(b), top.

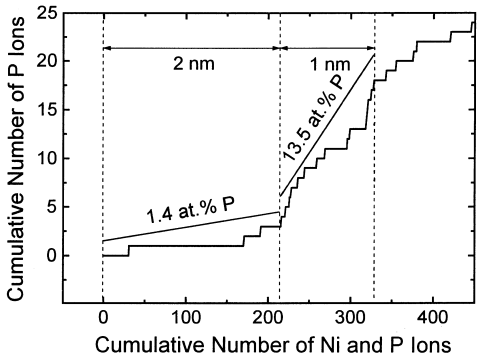

Fig. 4. Selected-area atom-probe analysis of as-plated Ni–3.6 at.% P, starting in the center of a grain. The integral profile shows a sharp transition from a region with low P content to a region with high P content.

After heat treatment C′, moderate grain growth

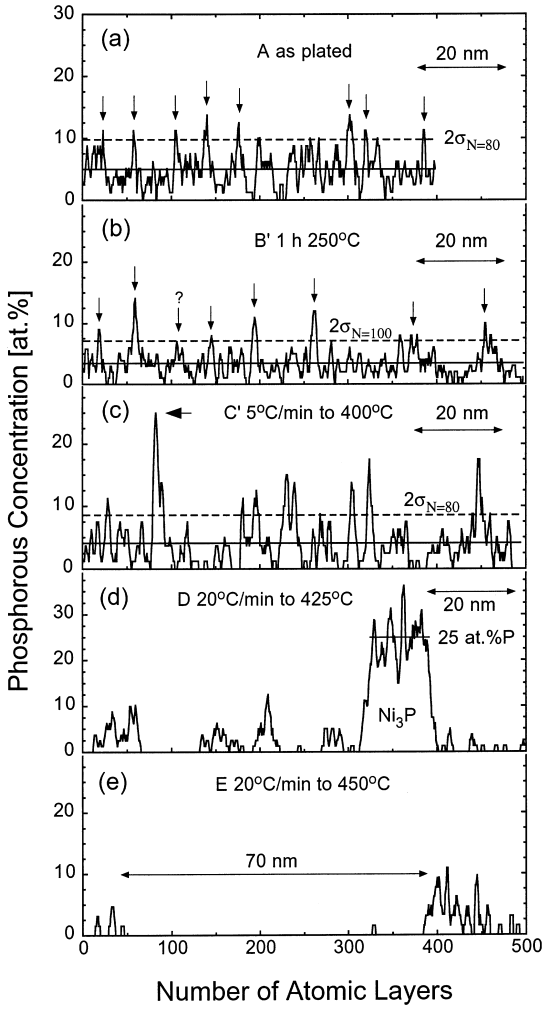

Fig. 5. Random-area atom-probe concentration profiles of initially nanocrystalline Ni–3.6 at.% P in different transformation stages: (a) as plated; (b) isothermally aged at 250°C for 1 h; (c) isochronally heated at 5°C/min to 400°C; (d) isochronally heated at 20°C/min to 425°C; (e) isochronally heated at 20°C/min to 450°C. Profiles (a), (b), (c), and (d) are smoothed with a moving average over four atomic layers. Solid lines indicate the average P concentration of the profile. Dashed lines mark the 2σ limits of the respective corresponding binomial distribution for a sample size of N ions, corresponding to four atomic layers.

can be detected in Fig. 3(c), top. The average grain diameter determined from the field-ion micrograph is 18 nm. This agrees well with the XRD result (22 nm) of state C, representing a slightly earlier transformation state. The concentration profile in Fig. 5(c), obtained on the C′ material, shows that the P distribution has changed considerably with respect to states A and B: the average height of the concentration peaks is 16 ± 4 at.% P, while the width of the segregation zone is still about 0.8 nm. The maximum P concentration detected is 25 ± 8 at.%. These results indicate (i) an increase of the P segregation at the grain boundary zones, and (ii) the nucleation of Ni_3P precipitates. The appearance of the Ni_3P phase after heat treatment C′ agrees exactly with the observation made by XRD on transformation state C.

The field-ion micrograph, Fig. 3(d), of a sample after heat treatment D exhibits marked grain growth with heat release II. In Fig. 5(d) a concentration profile obtained on D material is displayed. The presence of a large Ni_3P precipitate in the profile demonstrates that the Ni_3P phase formation has largely progressed. Sections of virtually pure Ni indicate that the supersaturation of the f.c.c. phase has been significantly reduced. Concentration peaks with 5–10 at.% P indicate that regions with P segregation are still present, however, with reduced segregation levels.

After heat treatment E, the microstructure is still nanocrystalline, but the grain size has substantially increased, Fig. 3(e). A concentration profile of material in state E, Fig. 5(e), shows the grains almost completely depleted in P. The length of the depleted section, about 70 nm, is approximately the size of the Ni grains determined by XRD.

4. DISCUSSION

The total enthalpy released ($\Delta H^{\exp}$) during the complete transformation of as-plated nanocrystalline Ni–3.6 at.% P layers to the microcrystalline equilibrium phases Ni(P) and Ni_3P amounts to $\Delta H^{\exp} = 3.3$ kJ/g-atom, as determined by DSC. We now discuss the respective enthalpy contributions of the observed structural and chemical changes during the transformation sequence.

First, for comparison, the heat release expected for a complete transformation of a hypothetical homogeneous supersaturated Ni–3.6 at.% P crystalline solid solution into the equilibrium phases is assessed. Using the free energies of the Ni–P system, as calculated by Ref. [4] based on experimental data with the CALPHAD method, a theoretical enthalpy release of $\Delta H^{\text{theo}} = 2.7$ kJ/g-atom results after subtracting the entropic contributions.

The AP and XRD results show, however, that the formation of Ni_3P occurs essentially during heat release II of the DSC thermogram, releasing only 1.1 kJ/g-atom. Because of the superimposed marked grain growth, this value gives an upper limit for the enthalpy release associated with the formation of Ni_3P. Considering these results, two conclusions can be drawn: (i) Ni_3P formation does not occur from a homogeneous solid Ni(P) solution; and (ii) if Ni_3P formation is attributed only to heat release II, the major part of the total transformation enthalpy, released during heat release I, must be related to other processes. The experimental results indicate structural and "chemical" relaxations, the former is a recovery of point defects and grain growth, and the latter segregation of P to grain boundaries.

Table 2. Transformation sequence of nanocrystalline Ni–3.6 at.% P. Heat releases I and II refer to the DSC thermogram displayed in Fig. 1. The sequence observed for amorphous Ni–P alloys with higher P contents [8, 9, 13] is given for comparison purposes

Heat release (DSC peak)	Transformation step	Nanocrystalline Ni–3.6 at.% P this work	Hypoeutectic amorphous Ni–x at.% P, $17 < x < 18$, Refs [8, 9, 13]
I	Ia	Structural relaxation	Structural relaxation
	Ib	Increase of P segregation and moderate grain growth	Formation of f.c.c. Ni crystallites
II	II	Formation of Ni_3P, grain growth	Bulk formation of crystalline Ni_3P, increase of the volume fraction of Ni

With this conclusion, the microstructural evolution during isothermal heating can be described as follows. In the as-plated state, the material is far away from the thermodynamic equilibrium. Structurally, it is characterized by numerous lattice defects in the crystallites, and, chemically, by an inhomogeneous P distribution with strong P segregation at grain boundaries of the nanocrystalline alloy. Heating to 250°C recovers most defects inside the grains, while the grain size and the chemical situation hardly change. This transformation is referred to in the following as transformation step I(a). The related enthalpy release during this first half of heat release I is roughly 1 kJ/g-atom. Heating the alloy to 400°C releases another 1 kJ/g-atom. This enthalpy change can be partly attributed to an enhancement of the P segregation at the grain boundaries up to the limit for nucleation of Ni_3P and partly to the beginning of grain growth. These microstructural changes are referred to as transformation step I(b) in the following. Finally, another 1 kJ/g-atom is dissipated in heat release II, when the vast part of Ni_3P is formed, superimposed on substantial grain growth. This latter transformation is called step II. The whole transformation sequence is summarized in Table 2.

A study of electrodeposited pure Ni with 10 nm grain size [19], containing 0.25 at.% S impurities, revealed a similar transformational behavior with two major heat releases upon isochronal heating. However, transformation step II of this alloy, related to substantial grain growth only, has already started at 290°C; that is more than 100°C below the observed threshold for the nanocrystalline Ni–3.6 at.% P alloys. This significant difference can be understood as an effect of P segregation drag; that is, the segregated P atoms must be carried along with the moving grain boundaries, thus inhibiting their mobility [20–22]. Furthermore, the driving force for grain growth, the interfacial free energy, is reduced in the case of Ni–P, as compared with pure Ni, due to the release of the segregation enthalpy. Hence, a solute addition like P can significantly enhance the thermal stability of a nanocrystalline microstructure.

In the following, we first compare the results of the present work with other studies of nanocrystalline and amorphous Ni–P alloys with higher P concentrations. Based on this, we outline a global picture of the microstructure and the transformation behavior of Ni–P alloys.

The observation of two distinct major heat releases related to three transformation steps upon heating is in accord with other studies of electroless plated as well as electrodeposited Ni–P alloys. A transformation sequence with transformation steps equivalent to steps I(a), I(b) and II of the present work has been reported for electroless plated nanocrystalline Ni–P with P contents between 3 and 13 at.% studied by dilatometry, electrical resistivity measurments, DSC, XRD, and TEM [13, 14]. Two major transformation steps were also found for electrodeposited Ni–P with P concentrations from 2 at.% to the eutectic concentration of about 19 at.% by TEM [11, 12] and DSC; see Ref. [8] and references therein. While the transformation temperature of the first major transformation step increases with P concentration, the peak temperature of the second major step was shown to decrease with increasing P concentration, until both characteristic transformation temperatures meet at about the concentration of the Ni(P)–Ni_3P eutectic at 19 at.% P; see Refs [8, 13, 14] and references therein. Furthermore, the microstructure has been found to change continuously with the average P concentration. Between 2 and about 10–12 at.%, the deposits have a nanocrystalline structure. In this concentration range, the average grain size decreases from about 10–15 nm to 2–4 nm [11, 13, 14, 23]. Within an intermediate concentration range, between about 10 and 15 at.% P, nanometer-sized crystallites are embedded in an amorphous matrix [4, 10]. Layers with about 12–13 to 20 at.% P were found to be amorphous [8, 9], and may contain a small volume fraction of crystallites [10]. Hence, there is no indication of a sharply defined critical P content separating nanocrystalline and amorphous alloys. It is worthwhile noticing that the continuous change of the as-plated microstructures upon changes in P content coincides with the smooth temperature variation of the two characteristic transformation temperatures of transformation steps I(b) and II. Also, the as-plated microstructure and the transformation sequence show the same characteristics for both electrodeposited and electroless plated alloys.

Schenzel [9] reports for an electroless plated, slightly hypoeutectic amorphous Ni–17.4 at.% P

alloy two microstructural transformations prior to the bulk crystallization upon isochronal heating at 5°C/min: first, at about 130°C, structural relaxation of the amorphous phase starts. Second, at about 260°C, crystalline f.c.c. nickel precipitates form within the amorphous matrix. These two processes coincide with the shallow peak of heat release I observed in the DSC thermogram of this alloy, as shown by Ref. [13]. The sharp peak of heat release II of the hypoeutectic alloy with an onset at 325°C is attributed to the formation of crystalline Ni_3P, accompanied by an increase of the volume fraction of f.c.c. Ni [9, 13]. The correlation of the transformation steps with the respective DSC peaks is also indicated in Table 2. The transformation of this hypoeutectic amorphous alloy thus follows the sequence

I(a): structural relaxation → I(b): Ni precipitation →

II: decomposition into Ni_3P + Ni.

In contrast, the relaxation step of hypereutectic amorphous Ni–20.2 at.% P is followed by the formation of Ni_3P crystallites without the preprecipitation of Ni crystallites [9]. Nickel crystallites could not be found by TEM and XRD even in the very first stages of transformation step II, even though Ni_3P and Ni form eventually together as step II proceeds [9]. Hence, the transformation sequence of the hypereutectic alloy can be summarized as

I: structural relaxation → II(a): Ni_3P precipitation →

II(b): decomposition into Ni_3P + Ni.

A comparison of the respective last two steps of these two transformation sequences reveals the characteristics of a eutectoid of the amorphous phase with the eutectoid concentration between 17.4 and 20.2 at.% P, very close to the eutectic concentration of the liquidus phase at 19 at.% P. The occurrence of an eutectoid means thermodynamically that the hypoeutectoid amorphous alloy does not have a driving force for Ni_3P formation until the P concentration has increased beyond the amorph-Ni_3P metastable equilibrium concentration by precipitating crystalline Ni solid solution and vice versa for the hypereutectoid alloy.

Based on the microstructures and transformation sequences reported in the literature for Ni–P alloys with P concentrations up to the amorphous range and the results of the present work for nanocrystalline Ni–3.6 at.% P, we outline in the following an overall description.

4.1. Microstructure of as-plated alloys

As the grain size decreases with increasing P content, the volume fraction of grain boundaries increases. At even higher P concentrations, Ni-rich crystallites embedded in an amorphous matrix and finally a completely amorphous alloy are found. This can be summarized in that first, at the cost of the crystalline phase, the volume fraction of the grain boundaries increases with the P content, then crystalline phase and grain boundaries are gradually replaced by the bulk amorphous phase. This suggests that the grain boundaries should be considered a separate phase, which is different from the crystalline and similar to the amorphous phase. The continuous transition with increasing P concentration can be accounted for simply by a gradually increasing volume fraction of the grain boundary (GB) phase, as given by a kinetically enforced, local, metastable equilibrium between Ni-rich f.c.c. and GB phase. A more quantitative description could be developed based on an estimation of a thermodynamic potential for the GB phase, e.g. by the CALPHAD method.

4.2. Transformation sequence

There are remarkable similarities between the transformation sequence of hypoeutectic amorphous Ni–17.4 at.% P

I(a): structural relaxation → I(b): Ni precipitation →

II: decomposition into Ni_3P + Ni

and the sequence observed in the present work for a nanocrystalline Ni–3.6 at.% P alloy

I(a): structural relaxation → I(b): P segregation →

II: Ni_3P phase formation.

The first and the third steps are essentially identical, as an increase in the volume fraction of Ni is certainly also related to transformation step II of nanocrystalline Ni–3.6 at.% P, even though hard to discern experimentally. The respective second step effects in both sequences the enrichment of P in the noncrystalline phase, amorphous in the former, and GBs in the latter sequence. The AP analyses of transformation state C′ of Ni–3.6 at.% P show that prior to the nucleation of Ni_3P, the P concentration within the GBs rises to about 16 at.% P, which is very close to the eutectic concentration. Based on these similarities between the transformation behavior of the GBs in the nanocrystalline and the hypoeutectic amorphous alloy, we propose a description of the formation of Ni_3P in the GBs with the concept of a eutectoid reaction as given above for the amorphous alloys. The analogy to an eutectoid implies that a driving force for the precipitation of Ni_3P in the GBs exists only if the P segregation exceeds a certain level.

An estimation of thermodynamic potentials for GB and amorphous phase can thus improve the understanding of the local P distribution in the

nanocrystalline alloy, the reduction of the GB interfacial energy due to segregation, and the transformation sequence upon heating. As the interfacial energy also represents the driving force for grain growth, this thermodynamic approach can provide, along with the possible segregation drag mechanism, an understanding of the thermal stability of nanocrystalline Ni–P.

5. SUMMARY

Atom-probe field-ion microscopy is employed for atomic scale investigation of the local distribution of P atoms in a nanocrystalline electroless plated Ni–3.6 at.% P alloy. The results demonstrate that P is segregated at the grain boundaries with a concentration as high as 11 at.% already in the as-plated state. The grains consist of a supersaturated Ni–P solid solution containing approximately 1 at.% P. Heating to 250°C recovers structural defects, while the grain size and chemical composition remain essentially unchanged. Isochronal heating to 400°C doubles the grain diameter from 9 to 22 nm and increases the P concentration in the segregation zone to 16 at.%. Also Ni_3P precipitates nucleate, presumably in the P-enriched grain boundaries. Substantial grain growth starts at 425°C. The Ni_3P phase formation is largely completed at 450°C. The underlying transformation sequence, structural relaxation → P segregation → Ni_3P phase formation, is very close to the transformation sequence known for amorphous Ni–P. This accounts for the similarity of the DSC curves of nanocrystalline and amorphous Ni–P, both exhibiting two exothermal peaks. A thermodynamic model is outlined which considers the grain boundaries in the nanocrystalline state as a separate phase similar to the amorphous phase. The observed microstructure and transformation sequence can be readily described by this model as being controlled by an initial, local, metastable thermodynamic equilibrium between a Ni-rich f.c.c. solid solution and a P-enriched grain boundary phase. The P enrichment of the grain boundaries is responsible for the comparatively high thermal stability of the nanocrystalline structure against coarsening.

Acknowledgements—Stimulating discussions with Professor D. N. Seidman, Northwestern University, are gratefully acknowledged. This manuscript was prepared for publication while Th.H. was with the Institut für Werkstoffwissenschaften V, Universität Erlangen-Nürnberg, Germany, and D.I. was with the Materials Science and Engineering Department, Northwestern University, Evanston, Illinois, and supported by the National Science Foundation, Division of Materials Research, and the Deutsche Forschungsgemeinschaft.

REFERENCES

1. Gleiter, H., *Prog. Mater. Sci.*, 1989, **33**, 223.
2. Rofagha, R., Erb, U. and Wood, D., *Can. Machinery Metalworking*, 1994, **89**, 29.
3. Erb, U., *Nanostruct. Mater.*, 1995, **6**, 533.
4. Lee, K. J. and Nash, P., in *Phase Diagrams of Binary Nickel Alloys*, ed. P. Nash. ASM International, Materials Park, OH, 1991.
5. Riedel, W., *Electroless Nickel Plating*. ASM International, Materials Park, OH, 1991.
6. Mallory, G. O. and Hajdu, J. B. (ed.), *Electroless Plating, Fundamentals and Applications*. American Electroplaters and Surface Finishers Society, Orlando, FL, 1990.
7. Kreye, H. and Gutmann, R., *Metalloberfläche*, 1993, **47**, 387.
8. Bakonyi, I., Cziraki, A., Nagy, I. and Hosso, M., *Z. Metallk.*, 1986, **77**, 425.
9. Schenzel, H.-G., *Microstructure and Corrosive Properties of Chemically Deposited Nickel–Phosphorus Layers with Nanocrystalline Structure*. VDI-Verlag, Düsseldorf, 1990, in German.
10. Dietz, G. and Schneider, H. D., *J. Phys.: Condens. Matter*, 1990, **2**, 2169.
11. Boylan, K., Ostrander, D., Erb, U., Palumbo, G. and Aust, K. T., *Scripta metall. mater.*, 1991, **25**, 2711.
12. Osmola, D., Nolan, P., Erb, U., Palumbo, G. and Aust, K. T., *Physica status solidi (a)*, 1992, **131**, 569.
13. Müller, F., *Production, Microstructure and Properties of Electroless Deposited Nickel–Phosphorus Layers with Nanocrystalline Structure*. VDI-Verlag, Düsseldorf, 1996, in German.
14. Kreye, H., Müller, F., Lang, K., Isheim, D. and Hentschel, Th., *Z. Metallk.*, 1995, **86**, 3.
15. Geber, G. P., Al-Kassab, T., Isheim, D., Busch, R. and Haasen, P., *Z. Metallk.*, 1992, **83**, 449.
16. Kubaschewksi, O. and Alcock, C. B., *Metallurgical Thermochemistry*, 5th edn. Pergamon Press, New York, 1979.
17. Knacke, O., Kubaschewski, O. and Hesselmann, K., *Thermochemical Properties of Inorganic Substances*, 2nd edn. Springer-Verlag/Verlag Stahleisen, Berlin/Düsseldorf, 1991.
18. Kissinger, H. E., *J. Res. natn. Bur. Stand.*, 1956, **57**, 217.
19. Klement, U., Erb, U., El-Sherik, A. M. and Aust, K. T., *Mater. Sci. Engng A*, 1995, **203**, 177.
20. Hu, H. (ed.), *The Nature and Behavior of Grain Boundaries*. Plenum Press, New York, 1972, p. 245.
21. Haasen, P., *Physikalische Metallkunde*, 2nd edn. Springer-Verlag, Berlin, 1984.
22. Haasen, P., *Physical Metallurgy*, 3rd edn. Cambridge University Press, Cambridge, 1996.
23. Allen, R. M. and Vandersande, J. B., *Scripta metall.*, 1982, **16**, 1611.